전력전자학술대회 논문집 2002. 7. 3 ~ 7. 6

소용량 전동기 구동용 새로운 IGBT 인버터 모듈

김만기, 장기영, 추병호, 이준배, 서범석, 김태훈
페어차일드 반도체 디스크리트 팀

A Novel IGBT inverter module for low-power drive applications

M.K. Kim, K.Y. Jang, B.H. Choo, J.B. Lee, B.S Suh, T.H. Kim
Discrete Team, PDD, Fairchild Semiconductor

ABSTRACT

This paper presents a novel 3-phase IGBT module called the SPM (Smart Power Module). This is a new design developed to provide a very compact, low cost, high performance and reliable motor drive system. Several distinct design concepts were used to achieve the highly integrated functionality in a new cost-effective small package. An overall description to the SPM is given and actual application issues such as electrical characteristics, circuit configurations, thermal performance and power ratings are discussed

1. Introduction

The terms energy-saving and quiet-running are becoming very important in the world of variable speed motor drives. Inverter technology is being increasingly accepted and used by a wide range of users in the design of their products. For low-power motor control, there are increasing demands for compactness, built-in control, and lower overall-cost. An important consideration, in justifying the use of inverters in these applications, is to optimize the total cost-performance ratio of the drive system.
In order to meet these needs, we have designed and developed a new series of compact, highly functional and very efficient power semiconductor devices called the SPM (Smart Power Module) . Fig. 1-(a) shows a real photograph of the SPM. SPM-inverters are a very viable alternative to conventional ones for low-power motor drives due to their attractive characteristics, specifically for appliances such as washing machines, air-conditioners etc. This paper describes in detail the design issues, electrical performance, and other important considerations for designing the system.

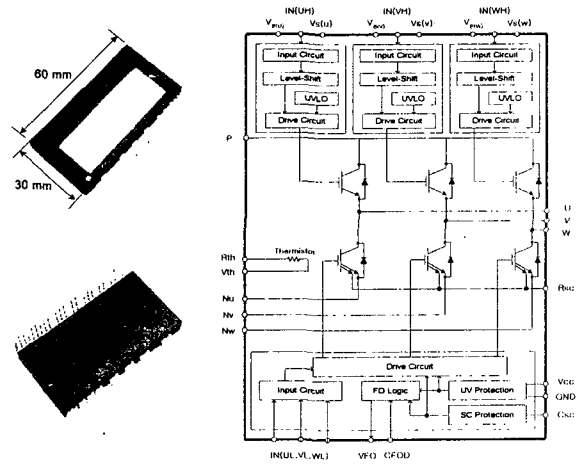

(a) Photograph of the SPM (b) Internal function block diagram

Fig. 1. Photograph of the SPM and the internal function block diagram.

2. Description of Design and Function Features

2.1 Features

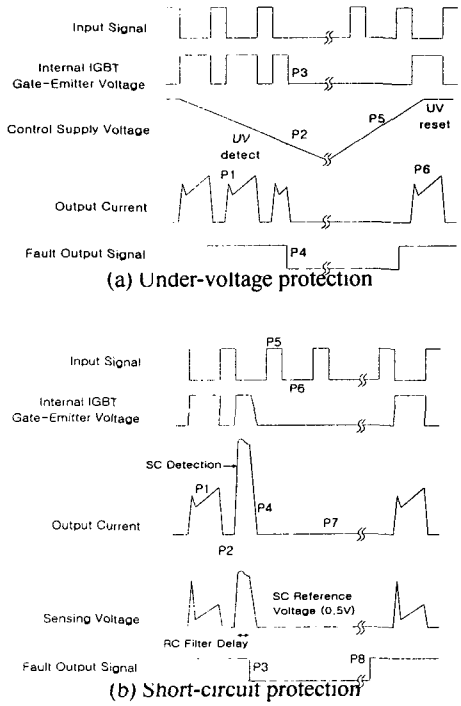

Fig. 2. Time chart of under-voltage and short-circuit protection.

The SPM combines optimized circuit protection and a drive that are matched to the IGBTs switching characteristics. The SPM is composed of three normal IGBTs, three sense IGBTs, three HVICs, one LVIC and one thermistor as shown in Fig. 1-(b). Highly effective short-circuit current detection /protection is achieved through the use of advanced current sensing IGBTs that allow continuous monitoring of the IGBT current. System reliability is further enhanced by the built-in over-temperature and integrated under-voltage lockout protection. The high speed built-in HVIC provides an opto-coupler-less IGBT gate driving capability that further reduces the overall size of the inverter system design. The HVIC facilitates the use of a single-supply drive topology. This allows the SPM to be driven by only one drive supply voltage without a negative bias. The SPM has three divided negative DC terminals to monitor the inverter output current by using three shunt resistors. Nowadays, the sensorless controlled inverter systems are widely used because of the advantages in drive cost, reliability and signal noise immunity. The SPM incorporates these terminals in order to provide a low-cost sensorless control solution[3].

2.2 Protective Functions

The SPM provides two main protective functions. One is control supply under-voltage protection and the other is short-circuit current protection. The principles of operation of these protective functions are described in the timing diagram in Fig. 2. When the control supply voltage drops under its UV detect level, the internal gating signal is blocked and a fault-out signal is generated. Once the supply voltage rises again over the UV reset level, the fault-out signal becomes high and the SPM is operated by the command signals. The LVIC of the SPM detects the low-side collector current level by monitoring the sensing voltage. In the case of a short-circuit, the SPM shuts down the internal gating signal and generates a fault-out signal. This current sensing method provides a simplified and cost-effective solution. The sense-IGBT has very linear sensing characteristics in the range of approximately above 15% of the rated current as shown in Fig. 4. Fig. 5 shows the real sensing voltage waveform. The sensing resistor, Rsc, can be selected to determine the trip current level which can be optimized according to the field requirements. Referto the overall application circuit of Fig. 10, which shows the Rsc and Rs parameters related to the short-circuit protection function. Fig. 3 and (1) show

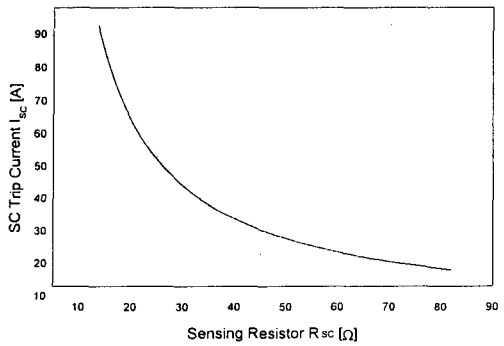

Fig. 3. The relatio nship between short-circuit trip current(Isc) and sensing resistor(Rsc).

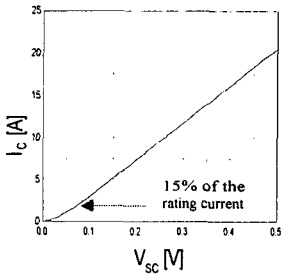

Fig. 4. Sensing characteristics of the sense-IGBT.

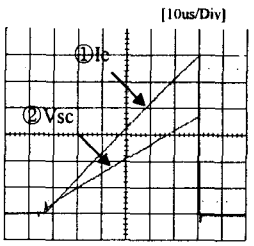

Fig. 5. Measured voltage in the sensing resistor, Rsc. Where,
① Collector current (5A/div.)
② Rsc voltage (0.2V/div.)

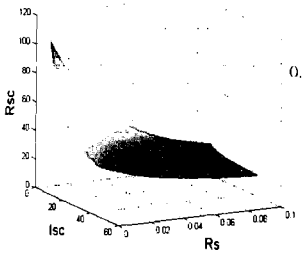

Fig. 6. Short-circuit trip current(Isc) related to sensing resistance(Rsc) and shunt resistance(Rs).

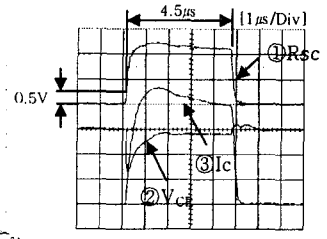

Fig. 7. Waveforms for short-circuit protection. Where,
① Rsc voltage (1V/div.)
② V_{CE} (100V/div.)
③ Collector current (20A/div.)

the relationship between the sensing resistor Rsc and the desired trip current Isc when the shunt resistor Rs is zero.

$$I_{SC} = 82 \times \frac{I_C\,(Rating\ Current)}{R_{SC}} \quad (1)$$

DUT : FSAM15SH60
where, I_{SC} : Circuit trip current [A]
R_{SC} : Sensing resistance [Ω]
I_C : Rating current of DUT [A]

The circuit trip current, Isc level is in inverse proportion to the Rsc value as shown in (1). We can see that the trip current level corresponding to the Rsc of 56Ω is 150% of the rated current. Isc level also decreases along with the increasing of the shunt resistor Rs. In case both Rsc and Rs are used, the relationship is shown in Fig. 6. Fig. 7 shows the actual waveforms under a short-circuit protecting situation with Rs=0Ω. The Rsc voltage increases as the low-side IGBTs collector current increases. Once the Rsc voltage in Fig. 10 reaches to 0.5V, the LVIC shuts down the gating signal after time delay of about 4.5us, which is mainly caused by a low-pass filter composed of Csc and Rf as shown in Fig. 10. Note that we wanted to detect 150% load current, with Rsc of 56Ω, which is around 24A, while using a 15A rated SPM.

3. ELECTRICAL CHARACTERISTICS AND PERFORMANCE

3.1 Electrical Characteristics

Table 1. shows the basic electrical characteristics of the FSAM15SH60. The table also includes theswitching loss data at Tj of 125℃ condition. This will be utilized for calculating the SPM power loss. Fig. 9 shows the switching waveforms of high-side, low-side IGBTs of the SPM under conditions shown in Table1.

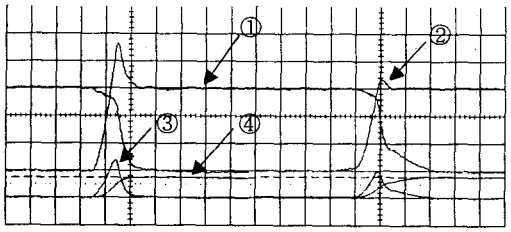

(a) High-side on/off switching waveform (100ns/Div)

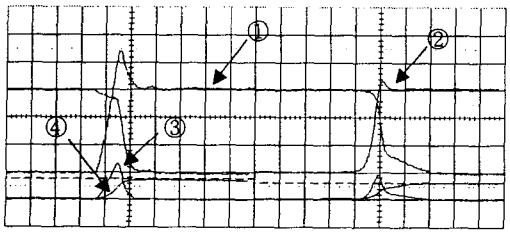

(b) Low-side on/off switching waveform (100ns/Div)

Fig. 9. High/Low side IGBT switching waveforms at Tj=25 ℃.
where, ① Ic (5A/Div.)
② V_{CE} (100V/Div.)
③ Switching power loss (4kW/Div.)
④ Switching energy (0.5mjoule/Div.)

3.2 Application Circuit and Design

The circuit configuration for a typicalapplication of the SPM is shown in Fig. 10. A single-supply 15V drives the low-side IGBTs directly and charges the bootstrap circuitry for the HVICs. The LVIC blocks the command signals from the controller and generates a fault signal when a failure mode, the SC current failure or the supply under-voltage failure, is detected.

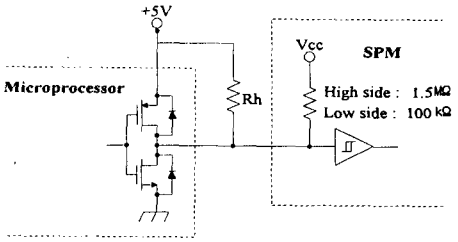

connection to a microprocessor.

The V_{FO} output is of the open-collector type. This signal line should be pulled up to the positive side of the 5V power supply with approximately 4.7kΩ. In the short-circuit protection circuit, the selection of the R_FC_{SC} time constant in the range of 3~4us is recommended. RF should be at least 30 times larger than R_{SC}. The integrated 5V CMOS/TTL compatible Schmitt trigger input conditioning circuit enables direct interface with a microprocessor. The high-side input is pulled up to +5V with a 1.5MΩ resistor and the low-side input is pulled up to Vcc with a 100kΩ resistor as shown in Fig. 11. When the driver part of the gate signal is composed of an open-collector, an appropriate pull-up resistor can be selected. When the driver part is composed with push-pull buffer, the low-side pull-up resistor is recommended to be under 2kΩ when Vcc is +15V. In order to increase the noise immunity, a pull-down capacitor can be used. The capacitances are recommended to be 1.2nF for the high-side and 0.47nF for the low-side

3.3 Thermal Performance and Operation Ratings

The power carrying potential of a device is dependent on the heat transfer capability of the device. The SPM provides not only good thermal performance but also operating frequency options in accordance with the application

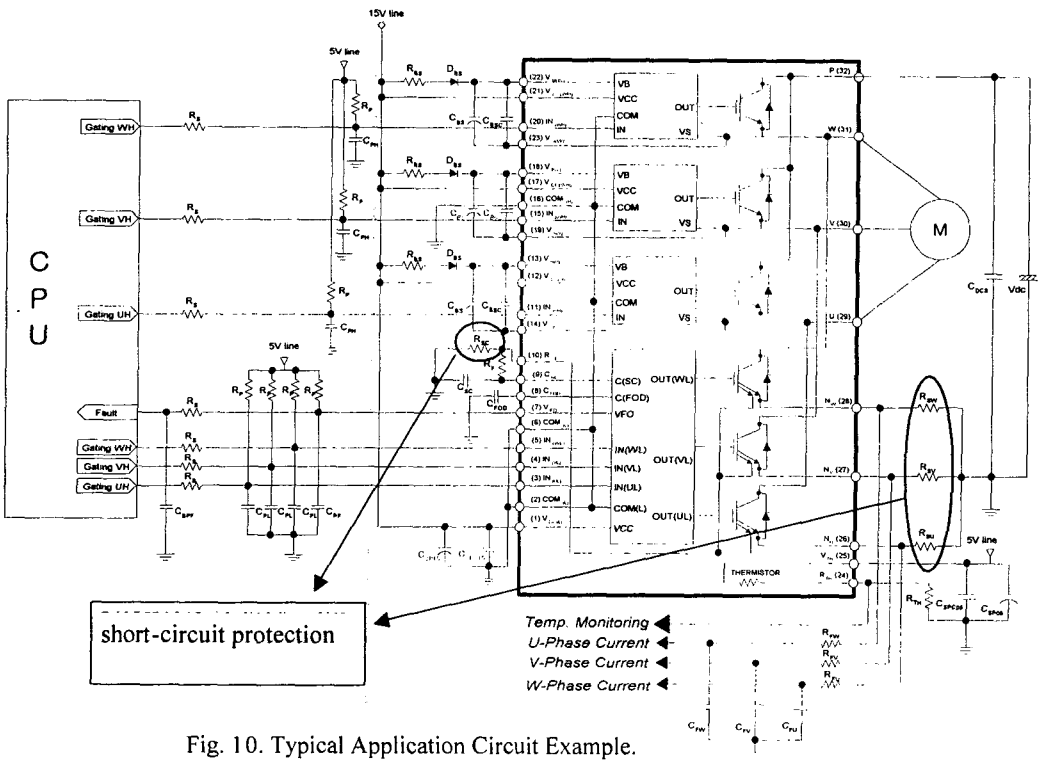

Fig. 10. Typical Application Circuit Example.

3.3.1 SPM power losses and ratings

The total power loss in the SPM is composed of conduction and switching losses caused in the IGBTs and FRDs. The loss during the turn-off steady-state can be ignored because it is a very small amount and has little effect on increasing the temperature in the device. The conduction loss depends on the DC electrical characteristics of the device i.e. saturation voltage. Therefore, it is a function of the conduction current and the device's junction temperature. On the other hand, the switching loss is determined by the dynamic characteristics like turn-on/off time and over-voltage/current. Hence, in order to obtain the accurate switching loss, we should consider the DC-link voltage of the SPM system, the applied switching frequency and the power circuit layout in addition to the current and temperature. For the detailed equations for calculating both conduction and switching losses based on a PWM-inverter system for motor control applications, refer to the references [4] and [5].

The typical forward characteristics of an IGBT and a diode can be measured by curve tracer equipment. Assuming that the switching frequency is high, the output current of the inverter can be considered as a sinusoidal one. That is,

$$i = I_{peak}\cos(\theta - \phi) \qquad (2)$$

where ϕ is a phase-angle difference between voltage and current. Using (2), the conduction loss of one IGBT and diode can be obtained. The switching energy loss Eon and Eoff can be measured by the switching waveform of a device. The switching loss depends on the IGBT and diode

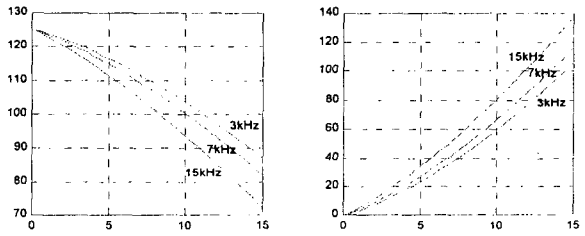

(a) SPM power loss (b) Allowable H/S temp.

Fig. 12. SPM power losses and allowable H/S temp. at 300Vdc.

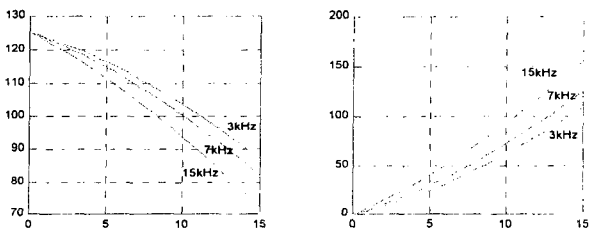

(a) SPM power loss (b) Allowable H/S temp.

Fig. 13. SPM power losses and allowable H/S temp. at 400Vdc.

is measured indirectly by multiplying the current and dynamic characteristics. The turn-off loss depends on the speed of the gate drive and the IGBTs current tail due to the recombination of minority carries. The turn-off energy voltage and integrating them over time. The turn-on loss is due to the rate of current change and the stored charge in the free wheel diode. The loss is measured using the same method. For the calculation of switching loss, the linear dependency of a switching energy loss on the switched current is assumed from the measurement result. The total nverter conduction losses are six times the Pcon of the IGBT and diode conduction losses. Fig. 12-(a) shows the calculated results including the total power loss due to conduction and switching in the IGBTs and FRDs. The results are obtained by using a high speed SPM device such as the FSAM15SH60. It should be noted that the PWM modulation index MI = 0.8 and $\cos\phi$=0.8 are used as common parameters in all the calculations. Figs. 12-(a) and 13-(a) show the power losses caused in the SPMs up to a rating current of 15A depending on the rms motor current variation. Fig. 12 shows the SPM power losses and acceptable maximum heatsink temperature to restrict the device s junction temperature below 125℃ at 300V of DC-link voltage. Fig. 13 shows a DC-link voltage of 400V. We can see that the difference of about 24% is in the power rating between 15kHz and 3kHz operating conditions. Fig. 14 shows a thermal impedance, which is the thermal resistance between junction and ambient air. The heat-sink used is shown in Fig. 15. When the DC-link voltage is 300V and Irms is 5A, the IGBT's power loss and FRD's power loss is 4.8W and 1.2W respectively. When thermal impedance is saturated, the difference in temperature of the junction and ambient air is:

$$\Delta T_{IGBT} = Z_{TH\_IGBT} \cdot P_{IGBT} = 20 \cdot 4.8 = 96°C$$

$$\Delta T_{FRD} = Z_{TH\_FRD} \cdot P_{FRD} = 74 \cdot 1.2 = 88.8°C$$

The junction temperature is:

$$T_{J\_IGBT} = \Delta T_{IGBT} + T_{AIR} = 96 + 40 = 136°C$$

$$T_{J\_FRD} = \Delta T_{FRD} + T_{AIR} = 88.8 + 40 = 128.8°C$$

The junction temperature is over 125℃. To keep the junction temperature below 125℃, it must stop operating at full power before around 1000 seconds.

3.4 Heatsink design guide

The selection of a heat-sink is constrained by many factors including set space, actual operating power dissipation, heat-sink cost, flow condition around a heat-sink, assembly location etc. In this paper, only some of the constraints are analyzed to give some insights in heat-sink selection from a practical application point of view.

Consider the type of heat-sink shown in Fig.15, which can be directly adopted for use in washing

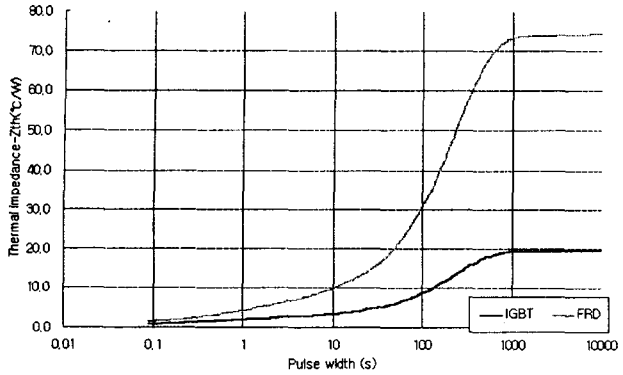

Fig. 14. SPM thermal impedance, junction-to-air (300V,40℃, Irms = 5A, fsw = 15kHz)

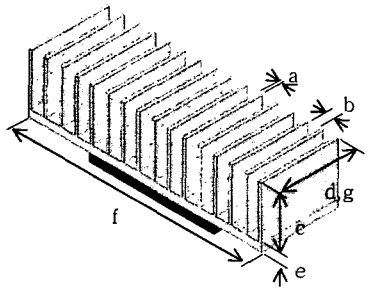

Fig. 15. A heat-sink example
a = Fin thickness(1.4mm), b = Fin spacing(6.0mm), c = Fin height(25mm), d = Fin length(37mm), e = Base-plate thickness(4.0mm), f = Base-plate width(112mm), g = Base-plate length(37mm)

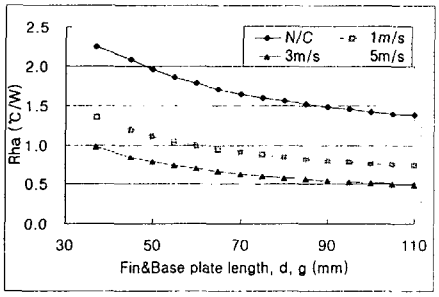

Fig. 16. Analysis results as heat-sink fin & plate length variation

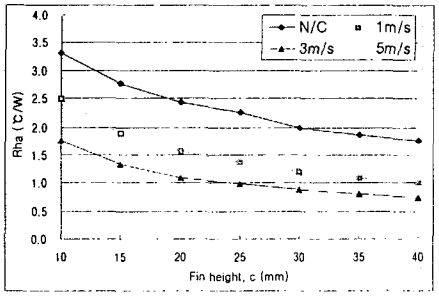

Fig. 17. Analysis results as heat-sink fin height variation

machines and modified for use in applications like air conditioners. Figs. 16 and 17 show the analysis results for the heat-sink-to-ambient thermal resistance, $R_{\theta ha}$, in designing the heat-sink. This varies widely with the changes in fin spacing, fin/base-plate length and fin/base-plate width. An increase in fin thickness decreases the total number of fins and the size of the heat-sink, resulting in an increase in thermal resistance.

Fig. 16 shows the results to see the effect of the base-plate length on thermal resistance. In the case where a cooling fan is not used, we can see that the increase in the length to 150%, that is 55.5mm (37mm(1.5), reduces the resistance to 82% (≅1.85℃/W), and an increase of 200% (37mm×2=74mm) reduces the resistance to 70.8% (≅1.6℃/W). Fig. 17 is the result of the variation in the fin height and it shows that the increase in the height to 150% (25mm ×1.5=37.5mm) reduces the resistance to 80% (≅1.8℃/W). The decrease in the height to 50% (25mm×0.5=12.5mm) increases the resistance to 135% (≅3.05℃/W). Therefore, increasing the height is more effective reducing the thermal resistance, as compared with increasing the length.

4. CONCLUSION

A novel 3-phase IGBT inverter module, the SPM (Smart Power Module), adopting a new ceramic-based transfer-molding technology, is introduced. Details of the main design concepts, functional capabilities and practical application issues are described. The SPM is targeted at low power inverter applications covering a power rating range up to 3kW at 220V ac input, resulting in smaller system size, higher reliability, and a better cost-performance ratio. With its unique technology, the SPM products will be expanded to cover wider power ranges and applications providing super compact device size in the very near future.

REFERENCES

[1] T. Yamada et al. "Next Generation Power Module," Intern. Symposium on Power Semiconductor Devices & IC's, Davos, Switzerland, 1994.

[2] Eric R, Motto, John F. Donlon, H. Iwamoto, "New Power Stage Building Blocks for Small Motor Drives," Power Electronics '99 Proceedings, pp.343-349, November, 99.

[3] Nobuyuki Matsui, "Sensorless PM Brushless DC Motor Drives," IEEE Transactions on Industrial Electronics, Vol. IE-43, No. 2, pp. 300-308, 1996, April.

[4] F. Casanellas, "Losses in PWM inverters using IGBT's," Proc. Inst. Elect. Eng.-Elect. Power Applicant. , vol. 141, no. 5, pp. 235-239, Sept.1994.

[5] K. Berringer, J. Marvin and P. Perruchoud, "Semiconductor Power Losses in AC inverters," Conf. Rec. of IEEE IAS'95, pp. 882-888, 1995

[6] Smart power module user's guide, application note AN9018, Fairchild Semiconductor